# Nonlinear Ion Acceleration for Improved Space Focusing in Time-of-Flight Mass Spectrometry

Ben D. Gardner
Department of Chemistry, Michigan State University, East Lansing, Michigan, USA

John F. Holland
Department of Biochemistry, Michigan State University, East Lansing, Michigan, USA

The initial spatial distribution of gas-phase ions is one of the primary factors limiting the achievable mass resolving power in time-of-flight mass spectrometry. While the effect of the spatial distribution is minimized along the flight path at a location known as the space-focus plane, the use of a single, linear acceleration field to generate this focus represents only a first-order approximation of ideal space focusing. Alternatively, ideal space focusing is possible through the use of a nonlinear ion acceleration field. A computational model delineates the requirements of the nonlinear potential profile, and suggests that substantial improvements to resolving power can be achieved when using an ion source configuration where a first field approximates the optimal nonlinear field gradient and a second, linear accelerating field imparts additional kinetic energy. Experimental results using a novel, static-field ion source geometry designed to allow selective position-specific ionization through photoinduced dissociation indicate that a 10× improvement in focusing can be achieved using this configuration. (J Am Soc Mass Spectrom 1999, 10, 1067–1073) © 1999 American Society for Mass Spectrometry

The utility of time-of-flight mass spectrometry (TOFMS) to applications requiring three-dimensional ionization or ion extraction volumes is hampered by characteristics of initial ion behavior that limit the mass resolving power. These are manifested in the initial ion population as spatial and energetic distributions and are fundamental in the analysis of gas-phase ions. For ions of a given *m/z*, the spatial distribution results in a range of final velocities as a consequence of the total acquired kinetic energy, which is a function of initial ion position at the moment of extraction. Likewise, the energetic distribution, which is a consequence of the range of initial thermal energies, also results in a velocity distribution, even for ions with the same *m/z* beginning at the same axial location.

The relative effect of these fundamental processes on resolving power depends on the application. For surface analysis techniques, where the spatial distribution is minimal, the energetic distribution is a primary limitation to resolving power. When the axial dimension of the ionization or extraction volume is relatively large, however, as is inherent with gas-phase analyses, the effect of the spatial distribution becomes more pronounced.

The first successful correction for the initial spatial distribution resulted primarily from the development of the two-field ion source by Wiley and McLaren [1]. Their developments brought recognition of a position along the flight path where the temporal distribution for ions of the same *m/z*, having originated from different locations within an ion source, is minimized—a position commonly known as the space-focus plane. Wiley and McLaren found that by using two-field acceleration in the ion source, the location for space focusing could be adjusted farther from the ion source and onto the detector at a distance which is a function of the two electric field strengths. While the low amplitude first accelerating field actually increased the temporal effect of the initial energy distribution, the ability to achieve both remote space focusing and an increase in the total flight time for all ions yielded an overall increase in mass resolving power. A second innovation of Wiley and McLaren attempted to compensate for the initial energy distribution by introducing a time delay between ionization and ion extraction. This process, known as time-lag focusing, essentially transformed the energy distribution of the ion population into a spatial distribution that was subsequently corrected by space focusing. The combination of time-lag and space focus-

Address reprint requests to John F. Holland, Department of Biochemistry, Michigan State University, East Lansing, MI 48824. E-mail: holland@pilot.msu.edu


1044-0305/99/$20.00
PII S1044-0305(99)00083-5

Received April 8, 1999
Revised May 28, 1999
Accepted June 5, 1999

ing yielded a significant increase in mass resolving power. Unfortunately, the optimal time lag was mass dependent, limiting the *m/z* range that could be simultaneously analyzed.

A more effective method for energy compensation has been the development of the ion mirror or reflectron [2–4] which provides mass-independent ion focusing. Significant improvements in mass resolving power have been achieved using the ion mirror, particularly for surface ionization techniques in which the initial spatial distribution is minimized. For gas-phase analyses, however, the gain in resolving power is much lower than that attained for surface analysis techniques because the ion mirror cannot distinguish between the spatially and thermally derived components of an ion's total energy. Consequently, the ion mirror cannot simultaneously provide complete temporal compensation for both the initial spatial and energetic distributions and is commonly optimized to provide partial compensation for each [5, 6].

For large three-dimensional ion sources, the initial spatial distribution is now the primary limitation to the achievement of increased mass resolving power. Unfortunately, space focusing using a linear ion acceleration field provides only a first-order approximation of ideal space focusing, and even under optimized conditions a temporal distribution due to initial ion position exists at the space focus plane. To achieve complete space focusing, a dynamic or static nonlinear acceleration field must be employed.

Several dynamic nonlinear field schemes have been proposed or implemented [7–10], whereby a uniform electric field is temporally varied beyond the ion source, generating a force that is effectively nonlinear in time. Here, ions with relatively lower velocity are subjected to the additional force for a longer time than their more energetic counterparts, reducing the arrival time distribution for iso-*m/z* ions. Static, parabolic nonlinear accelerating fields have also been developed where the space-focus plane is located at or close to the ion source exit [11–13]. However, only a portion of the ionization region imparts enough energy to ensure sufficient collisional energy at the detector surface. Additionally, the space-focus plane, and thus the detector, is located close to the exit of the accelerating field, and little time is available for additional *m/z* separation.

This report describes an alternative method of space focusing using a combination of nonlinear and linear static accelerating fields and describes a computational model for predicting the appropriate combination of linear and nonlinear fields for a given time-of-flight mass spectrometer. The nonlinear field provides compensation for the initial spatial distribution, whereas the subsequent linear field imparts additional energy to the ions and allows the space-focus plane to be located beyond the ion source exit. Results indicate that a significant increase in resolving power can be achieved using this ion optical configuration.

## Theory

### *Space Focusing Using Linear-Field Acceleration*

Space focusing depends on the fact that, in the presence of an electric field, an ion located closer to the exit in an ion source acquires less energy, and consequently a lower velocity, than an ion located farther back in the ion source. The less energetic ion exits the source first but is subsequently overtaken by the more energetic ion at the space-focus plane. Although the ion arrival time at the space-focus plane is a function of total ion energy and *m/z*, ideal space focusing requires that the arrival time be independent of initial ion position.

Consider the case of an ion accelerated from a single-field ion source. The time of flight to any position beyond the accelerating region may be determined by applying the basic equations for force and motion to yield eq 1,

$$t = \sqrt{\frac{2m}{z}}\left(\frac{(\sqrt{U_0 + esE_s} \pm \sqrt{U_0})}{eE_s} + \frac{D}{2\sqrt{U}}\right) \quad (1)$$

where the time of flight $t$, is a function of mass $m$, linear electric field strength $E_s$, the elementary unit of charge $e$, the number of unit charges $z$, distance $s$ between the ion and ion source exit, drift region distance $D$, ion thermal energy $U_0$, and total kinetic energy $U$. For this evaluation of initial position only, $U_0$ is taken to be 0. For two ions of the same *m/z* beginning from different axial positions $s_1$ and $s_2$ within the ion source, the time required for the more energetic ion to overtake the less energetic ion can be determined by rearranging eq 1 to solve for $D$ in each case, and subsequently setting the equations equal and solving for $t$:

$$t = \sqrt{\frac{2m}{zeE_s}}\frac{s_1 - s_2}{\sqrt{s_1} - \sqrt{s_2}} \quad (2)$$

It can be seen in eq 2 that the time to the space-focus position is dependent on initial ion position. It can similarly be shown, by solving for $D$, that the position at which the ions are coincident is also dependent on initial ion position. This dependence is a consequence of linear-field acceleration, which produces only a first-order approximation to ideal space focusing.

### *Nonlinear-Field Ion Acceleration*

The correct nonlinear potential profile required for complete space focusing in a time-of-flight mass spectrometer of a given focal length can be determined by evaluating a series of linear electric fields which, if relatively short in comparison to the overall ion source geometry, yield an effectively nonlinear electric field [14]. For the case where an additional relatively long linear accelerating field is included, the evaluation process is begun by first determining the linear accel-

erating field strength required to provide the expected time of flight to a remote detector for an ion of a given $m/z$ with no initial thermal energy, and initially located at the linear/nonlinear region boundary. Application of the basic equations for force and motion yields eq 3,

$$t = \sqrt{\frac{2m}{z}}\left(\frac{(\sqrt{U_0 + edE_d} + \sqrt{U_0})}{eE_d} + \frac{D}{2\sqrt{U}}\right) \quad (3)$$

where $E_d$ is the linear electric field strength and $d$ is the acceleration field length.

The nonlinear field is assumed to be a series of linear segments extending from the acceleration/ionization region boundary into the ionization region. The first field segment is calculated for the same ion used previously and the same expected time of flight, only beginning from a predetermined distance within the ionization region. The correct electric field strength ($E_{s_1}$) at the new location ($s_1$) must account for the fact that the ion will also be accelerated by the previously calculated electric field in the linear accelerating region. Incorporation of both electric fields yields eq 4.

$$t = \sqrt{\frac{2m}{z}}\left(\frac{(\sqrt{U_0 + es_1E_{s_1}} - \sqrt{U_0})}{eE_{s_1}} + \frac{(\sqrt{U_0 + e(dE_d + s_1E_{s_1})} - \sqrt{U_0 + es_1E_{s_1}})}{eE_d} + \frac{D}{2\sqrt{U}}\right) \quad (4)$$

Subsequent linear field segments are calculated in similar fashion for the same ion, beginning successively farther back in the ionization region, incorporating equations similar to eq 4 to determine the subsequent electric field segments and account for the fact that the ion will also be accelerated by each of the previously calculated electric fields. Expanding eq 4 to account for all fields, the final electric field in an ion source having $n$ fields of $x$ spacing can be determined using the equation

$$t = \sqrt{\frac{2m}{z}}\left[\sum_{i=1}^{n}\frac{\sqrt{U_0 + e\sum_{j=i}^{n}x_jE_j} - \sqrt{U_0 + e\sum_{k=i+1}^{n}x_kE_k}}{eE_n}\right] + D\frac{\sqrt{2m}}{2\sqrt{U_0 + \sum_{i=1}^{n}x_iE_i}} \quad (5)$$

where the indices $i$, $j$, and $k$ serve as computational counters. Equation 5 is merely an expansion of eq 4, and each electric field can be calculated with a simple computer program using a successive approximations algorithm to solve for the electric field being examined. The validity of this approach to nonlinear field determination has been verified by Yefchak [15].

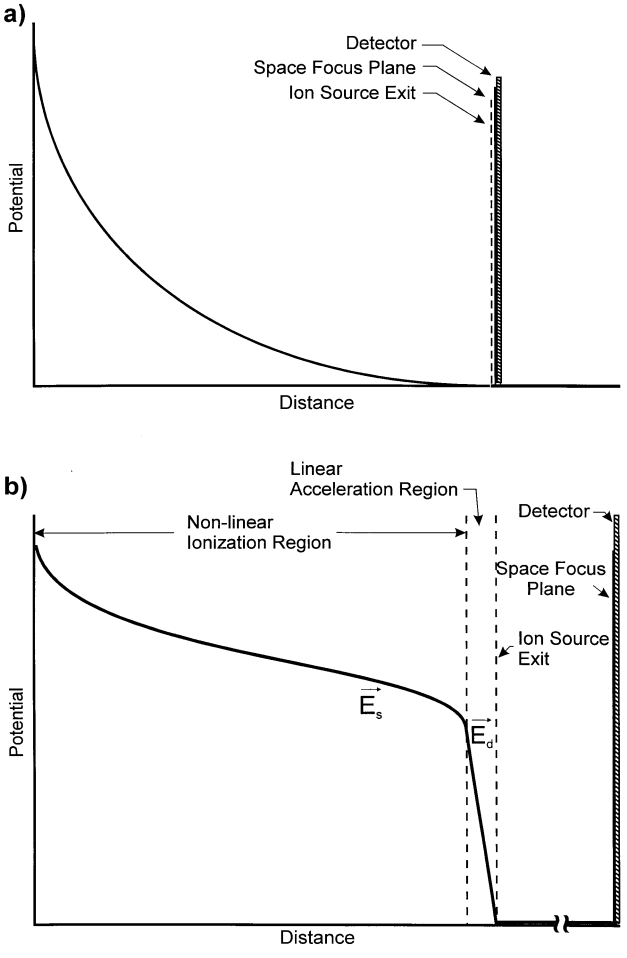


**Figure 1.** Potential profiles of the (**a**) nonlinear parabolic and (**b**) combined linear/nonlinear sigmoidal ion acceleration schemes.

The ideal electric potential profile using a nonlinear field alone is a parabolic function, illustrated in Figure 1. The addition of a subsequent linear accelerating field alters the electric potential profile of the nonlinear region to a sigmoid function. This perturbation from the parabolic function becomes more pronounced as the relative magnitude and field strength of the linear accelerating region increases. The sigmoidal profile is independent of $m/z$ and dependent on both the desired time of flight and the ion optical path length.

## Experimental

### *Mass Spectrometer*

A linear time-of-flight mass spectrometer was fabricated in house having an open-geometry ion source through which laser induced photoionization could be achieved at specific locations within the ionization

region of the source. The ion source housing was differentially pumped to minimize the flow of analyte molecules to the analyzer portion of the flight tube. An Einzel lens and deflection plate assembly was used to collimate and steer the ions beyond the ion source. The detector assembly was located 1.53 m beyond the ion source exit, and consisted of a 25-mm dual chevron microchannel plate assembly (Galileo). Data were acquired using a Tektronix TDS 620B, 500-MHz, 2.5-GS/s oscilloscope set to record a 16-transient moving average.

### *Ion Source*

The ion source consisted of multiple 7.6 cm diameter, 0.043 cm thick ring electrodes separated by 0.254 cm ceramic spacers except for a 0.076 cm thick spacer separating the accelerating region electrode and the first ionization region electrode. The overall length of the ionization region was 2.50 cm, and the acceleration region 0.65 cm. Each of the ionization region electrodes had a 4.45 cm diameter opening that was covered with 90% transmission electroformed grid material (MN-17, Buckbee-Mears St. Paul). The electrodes were electrically biased using a voltage divider circuit to generate a series of short, linear, electric field segments, configured to generate either linear fields or an approximation of nonlinear fields. A minimum accelerating field potential of 1600 V was required to achieve sufficient detector response, and thus served as the lower voltage limit for all experiments. The potential at the ion source back electrode was held at 1887 V during linear-mode operation.

### *Materials*

$Fe(CO)_5$ was obtained from Aldrich Chemical (Milwaukee, WI) and was chosen as the analyte due to its high ionization cross section and volatility at room temperature. Analyte vapor was introduced directly into the ion source housing from a sample vial attached to a direct probe interface assembly.

### *Laser and Optics*

Photoinduced dissociation of $Fe(CO)_5$ was achieved using a Quanta-Ray GCR-11 Nd:YAG laser, operating at $\lambda = 355$ nm, firing at 10 Hz with a 5-ns pulse duration. An optical rail, mounted on an ion source chamber flange, housed the beam guiding optical components that consisted of two high-reflection aluminum mirrors on adjustable mounts and a vertically oriented cylindrical lens on a fixed mount, as illustrated in Figure 2. The cylindrical lens focused the beam into a slit image that was narrow enough to pass between the ion source electrodes and increased the photon density in the space being targeted for ionization. The optical path was adjustable so as to place the focal line of the laser beam at the axial center of the ion source, while precisely positioning it along the ion optical axis to preselected points of ionization.

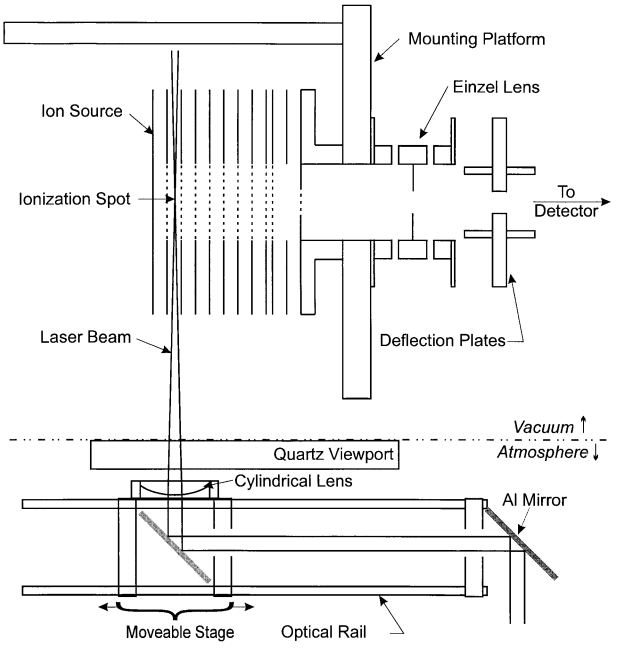


**Figure 2.** Instrumental configuration illustrating the open geometry ion source, subsequent ion optics, and adjustable laser targeting platform.

### *Calculation of Optimal Electric Field*

The calculated potential profile required to provide complete space focusing for the instrumental configuration described above was determined using eq 5 and is illustrated in Figure 3. The calculated ideal nonlinear field profile is a sigmoidal function, as expected. In this case however, the inflection point of this function is located beyond the back of the ion source.

## Results and Discussion

### *Linear Acceleration Model*

Three sets of data were collected with the ion source configured to provide the classical two linear electric fields at three different acceleration/ionization field ratios. The data correspond to the measured arrival time of the peak apex for *m/z* 56 ions. The theoretically predicted average arrival times of *m/z* 56 ions, along with the experimentally obtained data, are plotted in Figure 4 as a function of initial ionization location with respect to the ionization/acceleration field boundary and acceleration region potential. The theoretically derived traces exhibit a curvature due to the arrival time distribution expected when using a linear-field ion source configuration. The magnitude of this curvature is a function of the electric field ratio, which controls the axial location for space focusing. Curve A exhibits an

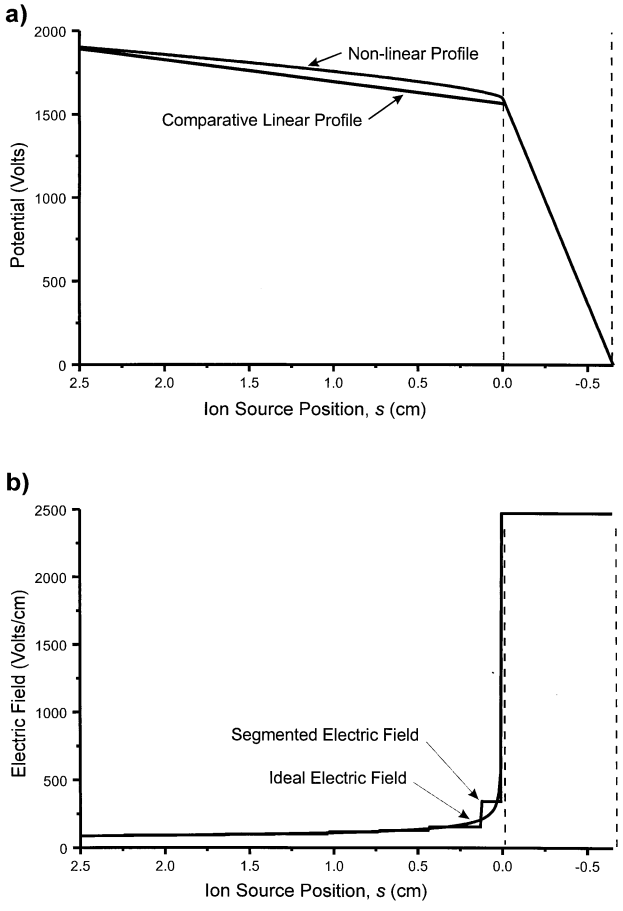


**Figure 3.** Nonlinear mode ion source configuration (**a**) potential profile and (**b**) electric field profile. Ion source position 0.0 cm denotes the location of the ionization/acceleration boundary. The distinction between the ideal and experimentally generated electric fields is most pronounced at the ionization/acceleration region boundary.

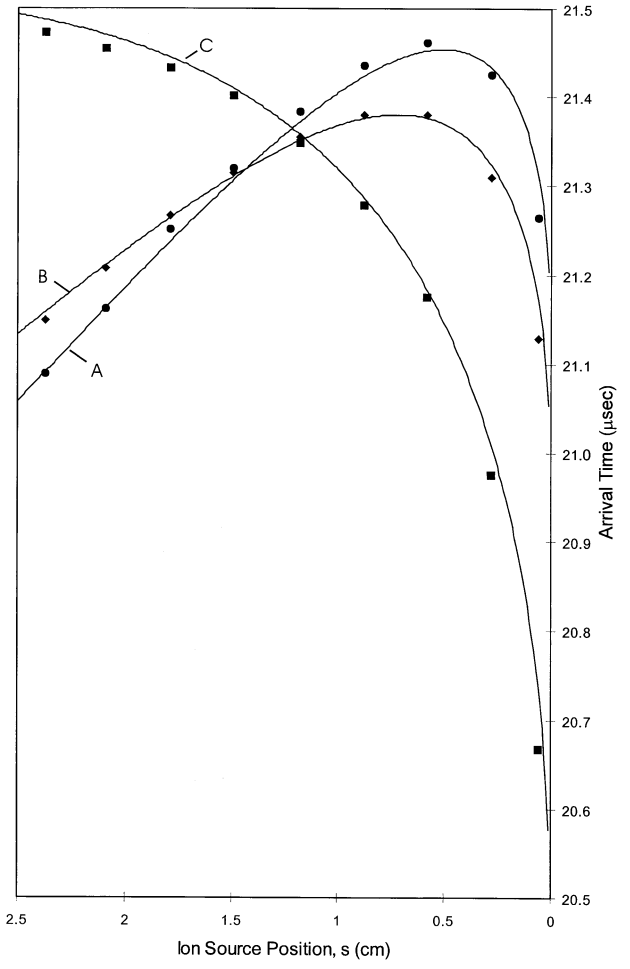


**Figure 4.** Theoretical and experimentally derived flight times for *m/z* 56 using experimental configuration operated in linear mode. Data sets A (filled square), B (filled circle), and C (filled diamond) correspond to acceleration/ionization region electric field ratios of 37.27, 24.36, and 21.96, respectively.

increase in ion arrival time as the initial position is moved back in the source, and is a consequence of the space-focus region being positioned beyond the detector surface. Curve B shows a generally opposite trend where, while the ion arrival time increases initially as the initial position moves back in the ionization region, a maximum arrival time occurs fairly close to the ionization region exit and the ion arrival time subsequently decreases as the initial position is located farther back in the source. This trend of ion arrival time decreasing with increased initial position is expected when space focusing occurs some distance before the detector location. The optimum ion arrival time distribution, shown as curve C, exhibits the minimum absolute arrival time range over the entire ionization region, with a total temporal distribution of 227 ns. This is achieved when the ion source electric field ratio is optimized, and corresponds closely to the optimal ratio predicted by Wiley and McLaren. In each case, the experimentally derived data agree closely in overall curvature with the theoretical prediction. This strongly supports the postulated first-order space-focus model and to our knowledge is the first data to confirm the predictions of ion behavior originally proposed by Wiley and McLaren.

## *Evaluation of Nonlinear Model*

The voltage profile used in the nonlinear ion source configuration was designed to provide an average ion arrival time similar to that obtained using the linear electric field configuration. A plot of the theoretically predicted and experimentally determined arrival times generated using the calculated required voltages is shown in Figure 5a. Ideally, there should be no deviation in ion arrival time due to initial ion location if the electric fields have been properly selected. The experimental data show an ion arrival time range of 63 ns, which is a 3.6× improvement in variance over the best case observed using linear electric fields. Minor empirical adjustment of several electrode voltages (1–2 V)

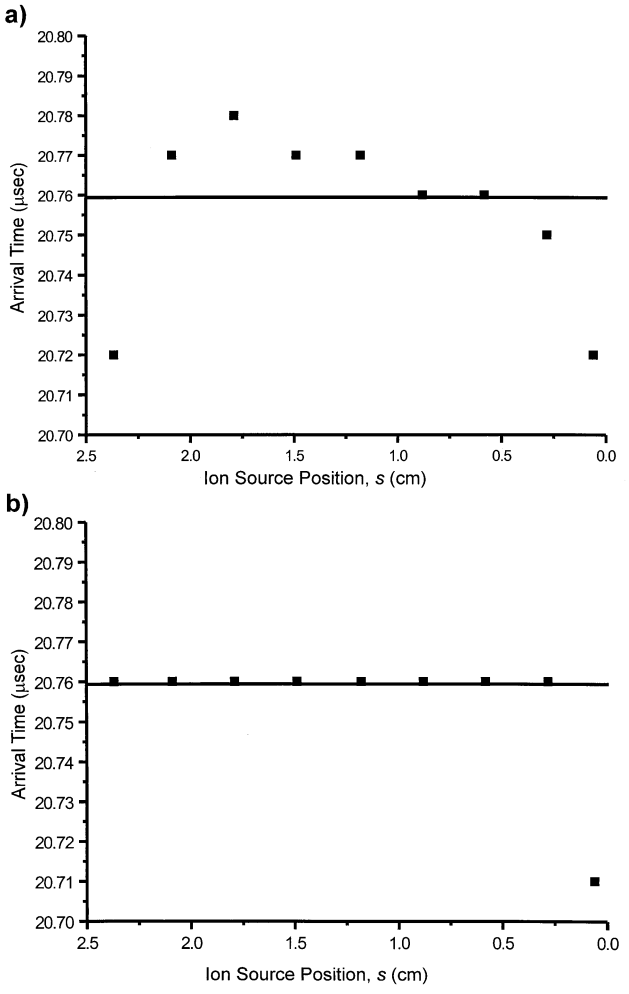


**Figure 5.** Ion arrival time distribution for *m/z* 56 ions using the (**a**) initial and (**b**) optimized nonlinear ion source configurations. The solid line denotes the expected arrival time.

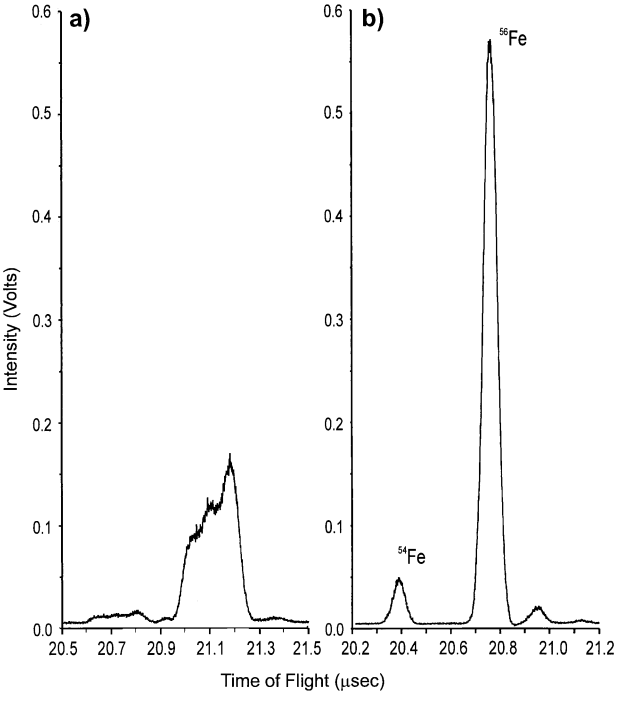


**Figure 6.** Integrated arrival time profile data obtained with both (**a**) linear and (**b**) nonlinear mode ion source configurations. The total ion current was similar for both cases.

improved the arrival time distribution to ~1 ns, as shown in Figure 5b, over all but the first ionization position, for which the narrowness of the electrode spacing interfered with laser beam focusing.

The contrast between linear and nonlinear ion acceleration over the extended ionization volume can be seen in Figure 6, which shows the summed arrival time profile, generated using the arrival time data of each ionization position, for both configurations. The reduced temporal distribution observed with the nonlinear configuration illustrates the performance enhancement achievable when the initial spatial distribution is eliminated as the primary constraint. Both the resolving power and signal intensity are improved. Elimination of the spatial distribution yields a significant improvement in performance, and the remaining temporal distribution is a function of other factors, including the initial thermal energy distribution, ionization time, collisional broadening, and dispersive effects of the grid mesh.

The ion source used in these experiments generates a series of homogeneous electric fields, which could be configured to provide either a single linear field over the ionization region or an approximation of a nonlinear field. Theoretically, a gridless electrode configuration could provide a completely nonlinear profile. However, initial experiments with this configuration exhibited a significant reduction in ion transmission. Computer modeling of the gridless design indicates that nonhomogeneity of the electric field across the source imparts a significant radial component to the ion trajectories. The use of multiple grids across the ionization region eliminates the radial nonhomogeneity.

The success of the utilized nonlinear configuration depends on the linear field segments being axially short relative to the ion source length, minimizing any electric field aberration. The range of ion arrival times theoretically expected for *m/z* 56 ions, beginning at any axial location within the ionization region of the experimental configuration, is plotted in Figure 7. Each linear field segment generates a range of arrival times depending on the precise axial initial position within the segment. However, the arrival time distribution predicted for the entire ionization region is less than that predicted using the single ionization field. For the segmented nonlinear configuration, the predicted temporal distribution due to the initial spatial distribution is reduced from 227 ns using the linear-mode configuration to 105 ns. The temporal distribution of the rear 80% of the ionization region is only 18 ns, which is a >10× improvement in space focusing over the linear-mode configuration.

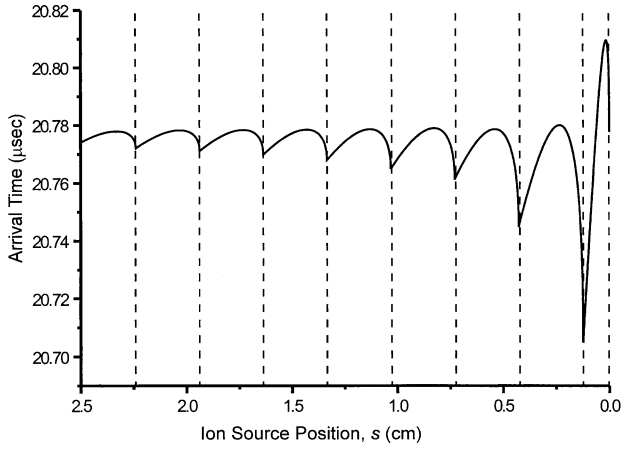


**Figure 7.** Theoretical arrival-time distribution expected for each field segment calculated for *m/z* 56 ions beginning from any axial position along the ionization region of the experimental configuration.

## Conclusions

The dependence of time of flight on initial ion position when using linear ion acceleration has been documented by experimental data using a two-field ion source model first described by Wiley and McLaren. These results, along with theoretical analysis, validate their claims that a linear ionization field provides a first-order approximation of space focusing. Theoretical calculations and experimental data also indicate that, for static field configurations, independence of time of flight on initial ion position requires the use of nonlinear acceleration. This may occur either exclusively or in concert with subsequent linear acceleration, so long as the nonlinear field is applied over the region spanning the axial range of initial ion positions. The concomitant use of linear and nonlinear fields combines the best features of the completely parabolic nonlinear model and the two-field linear model: the nonlinear field provides complete space focusing, and the combination of the two fields allows the space focus plane to be located beyond the end of the ion source. This flexibility cannot be achieved using either strictly nonlinear accelerating fields or two linear fields alone.

The use of nonlinear ion acceleration stands as a viable solution addressing instrumental configurations where the initial spatial distribution represents the primary limitation to achievable resolving power. While the effects of initial energy distribution are not addressed with nonlinear acceleration, a combination of nonlinear acceleration with energy correcting methods already described in the literature could provide additional enhancements to resolving power.

## Acknowledgments

The authors wish to thank Viatcheslav Artaev for helpful discussions in verifying the early version of the computational algorithm, and to the Michigan State University Mass Spectrometry Facility for financial support.

## References

1. Wiley, W. C.; McLaren, I. H. *Rev. Sci. Instrum.* **1955,** *26*, 1150.
2. Karataev, V. I.; Mamyrin, B. A.; Shmikk, D. V. *Sov. Phys. JETP* **1972,** *16*, 1177.
3. Mamyrin, B. A.; Karataev, V. I.; Shmikk, D. V.; Zagulin, V. A. *Zh. Eksp. Teor. Fiz.* **1973,** *64*, 82.
4. Mamyrin, B. A.; Shmikk, D. V. *Sov. Phys. JETP* **1979,** *49*, 762.
5. Glashchenko, V. P.; Semkin, N. D. *Sov. Phys. Tech. Phys.* **1987,** *32*, 665.
6. Short, R. T.; Todd, P. J. *J. Am. Soc. Mass Spectrom.* **1994,** *5*, 779.
7. Muga, M. L. *Anal. Instrum.* **1987,** *16*, 31.
8. Yefchak, G. E.; Enke, C. G.; Holland, J. F. *Int. J. Mass Spectrom. Ion Phys.* **1989,** *87*, 313.
9. Kinsel, G. R.; Johnston, M. V. *Int. J. Mass Spectrom. Ion Phys.* **1989,** *91*, 157.
10. Kinsel, G. R.; Mowry, C. D.; McKeown, P. J.; Johnston, M. V. *Int. J. Mass Spectrom. Ion Phys.* **1991,** *104*, 35.
11. Hulett, L. D., Jr.; Donohue, D. L.; Lewis, T. A. *Rev. Sci. Instrum.* **1991,** *62*, 2131.
12. Rockwood, A. L. *Proceedings of the 34th ASMS Conference on Mass Spectrometry and Allied Topics*, Cincinnati, OH, June 8–13, 1986; p 173.
13. Rockwood, A. L.; Udseth, H. R.; Gao, Q.; Smith, R. D. *Proceedings of the 42nd ASMS Conference on Mass Spectrometry and Allied Topics*, Chicago, IL, May 29–June 3, 1994, p 1038.
14. Gardner, B. D.; Artaev, V. B.; Holland, J. F. *Proceedings of the 43rd ASMS Conference on Mass Spectrometry and Allied Topics*, Chicago, IL, May 29–June 3, 1994, p 1040.
15. Flory, C. A.; Taber, R. C.; Yefchak, C. E. *Int. J. Mass Spectrom. Ion Phys.* **1996,** *152*, 169.